SOFT ROBOTICS Volume 00, Number 00, 2022 © Mary Ann Liebert, Inc. DOI: 10.1089/soro.2021.0008



Open camera or QR reader and scan code to access this article and other resources online.



Leaf-Like Origami with Bistability for Self-Adaptive Grasping Motions

Hiromi Yasuda,^{1,2,*} Kyle Johnson,^{3,*} Vicente Arroyos,³ Koshiro Yamaguchi,¹ Jordan R. Ranev,² and Jinkyu Yang¹

Abstract

The leaf-like origami structure is inspired by geometric patterns found in nature, exhibiting unique transitions between open and closed shapes. With a bistable energy landscape, leaf-like origami is able to replicate the autonomous grasping of objects observed in biological systems such as the Venus flytrap. We show uniform grasping motions of the leaf-like origami, as well as various nonuniform grasping motions that arise from its multitransformable nature. Grasping motions can be triggered with high tunability due to the structure's bistable energy landscape. We demonstrate the self-adaptive grasping motion by dropping a target object onto our paper prototype, which does not require an external power source to retain the capture of the object. We also explore the nonuniform grasping motions of the leaf-like structure by selectively controlling the creases, which reveals various unique grasping configurations that can be exploited for versatile, autonomous, and self-adaptive robotic operations.

Keywords: origami, grasping robots, bistability

Introduction

PLANTS AND ANIMALS are perpetually subjected to the unpredictable nature of their ever-changing surroundings, forcing the development of dynamic responses and self-adaptive behavior to accommodate for their rapidly changing environment. For example, sea anemones can catch targets with different shapes and sizes because of their self-adaptive morphology, and the Venus flytrap is capable of self-adaptive movements in response to a multitude of stimuli. Engineering a versatile grasping device that can mimic the nastic movements of these natural adaptive systems is one of the many challenges facing the field of robotics.

Recently, origami-inspired structures have been studied with a focus on biomimetic folding/unfolding behavior. For example, one of the most well-known crease patterns, the Miura-ori, ⁴ can be found in tree leaves and other plants. ^{5–7} In addition, a fast folding grasping motion inspired by earwig wings has been demonstrated by introducing an extensional membrane element to the Miura-ori building block. ⁸ These Miura-ori-based reconfigurable structures show great potential for engineering devices, but the variations of their folding patterns are still limited to the single degree-of-freedom (DOF) nature of the Miura-ori fold implemented using a rigid origami approach. These limitations have hindered the adoption of Miura-ori in practical applications.

¹Department of Aeronautics & Astronautics, University of Washington, Seattle, Washington, USA.

²Department of Mechanical Engineering and Applied Mechanics, University of Pennsylvania, Philadelphia, Pennsylvania, USA.

³Department of Electrical and Computer Engineering, University of Washington, Seattle, Washington, USA.

^{*}These two authors contributed equally to this work.

Using the Miura-ori unit cell as a building block, De Focatiis and Guest explored the biomimetic leaf-like origami patterns, specifically leaf-in and leaf-out origami⁶ (see Fig. 1 for the leaf-out origami in which its Miura-ori unit cells are directed outward⁶; also see Refs.^{6,9} for the leaf-in origami whose unit cells are directed inward). It has been shown that leaf-out origami can exhibit numerous rigid folding motions (i.e., multi-DOF) despite the single DOF nature of the individual Miura-ori elements.⁹ Another interesting aspect of the leaf-out origami structure is its tunable bistability.

While these studies have shown versatile characteristics of leaf-out architectures, a systematic investigation on leaf-out origami kinematics needs to be yet conducted, particularly with the focus on transition between multistable configurations, tunable energy landscape, and the development of numerical framework to calculate various folding/unfolding motions.

Also, from the engineering standpoint, the applications of leafout origami have been largely unexplored despite such versatile morphology and stability characteristics.

Here, we demonstrate the feasibility of using leaf-out origami's reconfigurability and bistability to achieve versatile, autonomous, and self-adaptive grasping motions. First, we use a rigid origami model to characterize the unique kinematics of the structure, especially transitions between open and closed modes separated by the flat state. In addition, we model the crease folding as a torsional spring (e.g., waterbomb origami^{10,11} and degree-4 vertex origami¹²), and we examine the ability to tailor the energy landscape by altering the design parameters, specifically the rest angle of the spring element. We then design and fabricate multilayered prototypes of the leaf-out origami structure with tailored energy barriers.

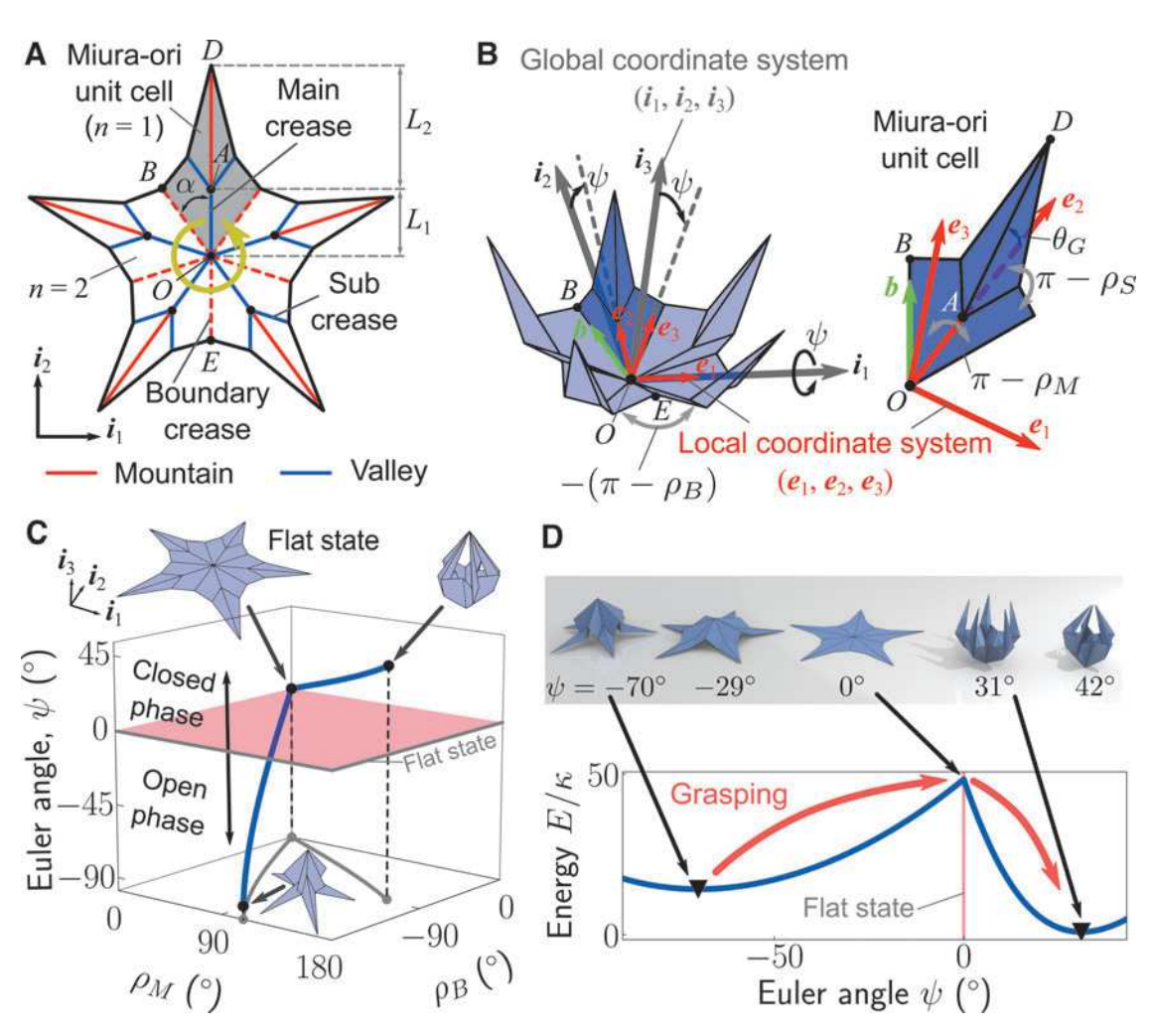


FIG. 1. Leaf-out origami for grasping objects based on bistability. (**A**) Flat configuration of the leaf-out origami composed of five Miura-ori unit cells. *Red* (*blue*) *lines* indicate mountain (valley) crease lines. *Dashed lines* indicate the mountain boundary crease lines connecting adjacent Miura-ori unit cells. (**B**) Folded configuration of the leaf-out origami. We define the global coordinate as well as the local coordinate attached to one of the Miura-ori unit cells. The folding angle along the boundary crease is defined as ρ_B . *Right inset* illustrates the geometry of the Miura-ori unit. We define two folding angles ρ_M and ρ_S for the main and subcrease lines, respectively. (**C**) The uniform grasping motion of the leaf-out origami is plotted in the configuration space. The folding path projected onto the bottom plane ($\rho_M \rho_B$ -plane) is denoted by the *gray line*. (**D**) The leaf-out origami can exhibit bistable behavior *via* transformation from its folded shape (open phase) into another folded configuration (closed phase) passing through the flat state. ($\bar{\rho}_M$, $\bar{\rho}_B$) = (120° - 30°) is used for this calculation. Color images are available online.

We experimentally demonstrate the feasibility of catching a falling object by triggering the grasping motion, which only occurs within a predetermined range of impact forces. Furthermore, we numerically explore various grasping configurations by controlling selected Miura-ori unit cells. Our numerical analysis reveals the multitransformable morphology of the leaf-out origami. This is demonstrated through the simulation of distinct grasping movements: a two-fingered pinching motion and a symmetric four-fingered grasping motion.

Our grasping mechanism has advantages over other designs in that the leaf-like origami structure can be easily tailored, fabricated, and actuated for various mechanical properties and applications. ^{13–15} That is, multistable and multitransformable devices can be manufactured only from surface materials, which leads to fast 2D machining (e.g., laser cutting) and simple and lightweight systems.

Although multistable mechanisms (especially bistable behavior) have been previously used to design and actuate various robotic devices such as grippers, ^{16–18} swimming robots, ¹⁹ and jumping robots, ²⁰ they tend to be complicated, and/or induce cumbersome fabrication processes. Based on the tunable dynamic response of the origami-based structure, our design principles demonstrate great potential for designing and fabricating simple robot prototypes to create devices for various applications such as surgical robots, space, deployable structures, and catch-and-release traps.

Materials and Methods

Leaf-out origami model

The leaf-out origami consists of $n_{\rm cell}$ Miura-ori unit cells (Fig. 1A), with neighboring unit cells connected by the boundary crease lines. ^{6,9} The Miura-ori is known as a rigid origami structure whose surfaces can be modeled as rigid panels connected by hinges, and exhibits 1 DOF folding motion. The geometry of each Miura-ori unit cell is characterized by the following geometrical parameters: central angle $(\alpha = \pi/n_{\rm cell})$ and length parameters $(L_1 = \overline{OA})$ and $(L_2 = \overline{AD})$. Based on the 1 DOF nature of the Miura-ori unit cell, the folding motion of the whole leaf-out origami can be expressed by considering the orientation and folding motion of each Miura-ori unit cell.

To describe the orientation of the unit cell, we introduce the global coordinates ($R_I = [i_1 \ i_2 \ i_3]$) and the local coordinates ($R = [e_1 \ e_2 \ e_3]$) attached to the Miura-ori unit cell such that the e_2 -axis is aligned with \overline{OA} and the direction of e_3 is the same as the i_3 -axis at the flat state (Fig. 1B). By using these coordinate systems, we define the Euler angle (ψ) to express the rotation of the local coordinate system (R) around the i_1 -axis as $R = R_I R_1$ where

$$\mathbf{R}_1 = \begin{bmatrix} 1 & 0 & 0 \\ 0 & \cos \psi & -\sin \psi \\ 0 & \sin \psi & \cos \psi \end{bmatrix}. \tag{1}$$

Here, if the leaf-out origami shows uniform grasping motion, the negative and positive Euler angles ψ indicate the open and closed states, respectively, as shown in Figure 1C. We later discuss the details of this uniform grasping motion.

Let n be the unit index numbered counterclockwise. To analyze the folding motion of the nth Miura-ori unit cell, we use the two folding angles, $\rho_{M,n}$ along the main crease lines and $\rho_{S,n}$ along the subcrease lines, with relationships between these two folding angles as follows:

$$\tan(\theta_G/2) = \tan \alpha \sin(\rho_M/2) \tag{2.1}$$

$$\sin(\theta_G/2) = \sin \alpha \sin(\rho_S/2) \tag{2.2}$$

where θ_G is an angle between e_2 and a vector pointing from Vertex A to Vertex D, as shown in Figure 1B. The folding angle for the boundary crease, connecting the nth and the (n+1)th unit cells, is denoted by $\rho_{B,n}$. Here, the folding angle (ρ_j) along the crease line j is defined as the complement of the angle between adjacent surfaces connected by the crease j, so that the positive and negative folding angles indicate valley and mountain folds, respectively. In this study, we assume that the leaf-out origami maintains its mountain and valley crease assignments during folding/unfolding motions, that is, $0 \le \rho_M$, $\rho_S \le \pi$ and $-\pi \le \rho_B \le 0$. We also examine the relationship between the folding angle ρ_B and the Euler angle ψ . We consider the unit vector $\mathbf{b} = [b_1 \ b_2 \ b_3]^T$ along the boundary crease OB, as shown in Figure 1B, which is expressed by

$$b = [i_1 \ i_2 \ i_3] \begin{bmatrix} -\sin\alpha\cos(\rho_M/2) \\ \cos\alpha\cos\psi - \sin\alpha\sin\psi\sin(\rho_M/2) \\ \cos\alpha\sin\psi + \sin\alpha\cos\psi\sin(\rho_M/2) \end{bmatrix}. \quad (3)$$

To analyze the unique multitransformable feature of the leaf-out structure, 9 we use the rigid origami simulation technique 21,22 and explore various grasping motions. We briefly review the rigid origami simulation technique 21,22 in this section. First, we consider the loop closure constraint around vertex O, which is connected to $N=2n_{\rm cell}$ creases (see the yellow arrow in Fig. 1A): $F(\rho_O)=\chi_1\chi_2\cdots\chi_N=I_3$ where I_m is the $m\times m$ identity matrix, and $\rho_O=\left[\rho_{M,1}\rho_{B,1}\cdots\rho_{M,n_{\rm cell}}\rho_{B,n_{\rm cell}}\right]^T$ is the vector composed of N folding angles along crease lines connected to vertex O. χ_j represents the rotation matrix for the crease j as a function of the folding angle ρ_j and the central angle α (Fig. 1A):

$$\chi_{j} = \begin{bmatrix} \cos \rho_{j} & 0 & \sin \rho_{j} \\ 0 & 1 & 0 \\ -\sin \rho_{j} & 0 & \cos \rho_{j} \end{bmatrix} \begin{bmatrix} \cos \alpha & -\sin \alpha & 0 \\ \sin \alpha & \cos \alpha & 0 \\ 0 & 0 & 1 \end{bmatrix}. \quad (4)$$

Then, if we take a derivative of F with respect to ρ_j , we obtain

$$\frac{\partial \mathbf{F}}{\partial \rho_1} \Delta \rho_1 + \dots + \frac{\partial \mathbf{F}}{\partial \rho_j} \Delta \rho_j + \dots + \frac{\partial \mathbf{F}}{\partial \rho_N} \Delta \rho_N = \mathbf{0}$$
 (5)

where $\Delta \rho_j$ is an increment folding angle, and the partial derivative is calculated as

$$\frac{\partial \mathbf{F}}{\partial \rho_j} = \begin{bmatrix} 0 & -a_j & c_j \\ a_j & 0 & -b_j \\ -c_j & b_j & 0 \end{bmatrix}. \tag{6}$$

Note that this matrix consists of only three independent variables a_j , b_j , and c_j , instead of nine. By using this partial derivative, we can rewrite Equation (5) as $C\Delta\rho = 0$ where $\Delta\rho = \left[\Delta\rho_{M,1} \ \Delta\rho_{B,1} \ \cdots \ \Delta\rho_{M,n_{\text{cell}}} \ \Delta\rho_{B,n_{\text{cell}}}\right]^T$, and

$$\mathbf{C} = \begin{bmatrix} a_1 & a_2 & \cdots & a_N \\ b_1 & b_2 & \cdots & b_N \\ c_1 & c_2 & \cdots & c_N \end{bmatrix}. \tag{7}$$

Therefore, the solution is calculated as follows:

$$\Delta \rho = [\mathbf{I}_N - \mathbf{C}^+ \mathbf{C}] \Delta \rho_0 \tag{8}$$

where C is the global linearized constraint matrix, and C^+ is the Moore/Penrose pseudoinverse matrix of C. However, through the iterations of each folding step in the simulations based on the Euler integration, the residual $F(\rho^{(0)} + \Delta \rho) - I_3$, where $\rho^{(0)}$ indicates the initial valid folding angle, is accumulated. Here, we define $\mathbf{r} = \begin{bmatrix} r_a & r_b & r_c \end{bmatrix}^T$, which is composed of the residual components calculated from

$$F(\rho^{(0)} + \Delta \rho) = \begin{bmatrix} 1 & 0 - r_a & 0 + r_c \\ 0 + r_a & 1 & 0 - r_b \\ 0 - r_c & 0 + r_b & 1 \end{bmatrix}.$$
 (9)

Then we modify Equation (8) by introducing an additional term to compensate for the accumulation of numerical error as follows^{21,22}:

$$\Delta \boldsymbol{\rho} = [\boldsymbol{I}_N - \boldsymbol{C}^+ \boldsymbol{C}] \Delta \boldsymbol{\rho}_0 - \boldsymbol{C}^+ \boldsymbol{\xi}. \tag{10}$$

In this study, we determine ξ by numerically solving $r(\rho^{(0)} + \Delta \rho, \xi) = 0$.

To control the folding angle of a desired crease line, we alter $\Delta \rho_0$ and embed the condition for the controlled crease line in Equation (10). If we control the folding angle of crease line j (here, we use $\Delta \rho_C$ for controlled angle increment), we modify $\Delta \rho = [\Delta \rho_1 \cdots \Delta \rho_j \cdots \Delta \rho_N]^T$ as $\Delta \rho = [\Delta \rho_1 \cdots \Delta \rho_C \cdots \Delta \rho_N]^T$. Also, to implement the controlled crease line in $K = I_N - C^+C$, we impose the K(j, :) = 1, that is, the components of the matrix K in the jth row are zero, except K(j, j) = 1.

Based on the rigid origami simulation, we conduct the energy analysis by modeling crease line j of the leaf-out origami as a linear torsion spring with spring constant κ_j (Supplementary Fig. S1). By using this torsion spring model, we analyze the energy landscape as follows:

$$E = \frac{1}{2} \sum_{j=1}^{N_{\text{Total}}} \kappa_j \left(\rho_j - \bar{\rho}_j \right)^2, \tag{11}$$

where N_{Total} is the total number of crease lines in the leaf-out origami, and $\bar{\rho}_i$ is the rest folding angle of *j*th crease line.

Fabrication of the paper prototypes

To empirically test the leaf-out structure, we fabricate a multilayered structure to enhance the rigidity of each facet, as well as the folding behavior of the crease lines, which achieves rigid origami-like folding motions, that is, deformation only takes place along the crease lines. We utilize a CO_2 laser system to fabricate our prototypes. Figure 2A

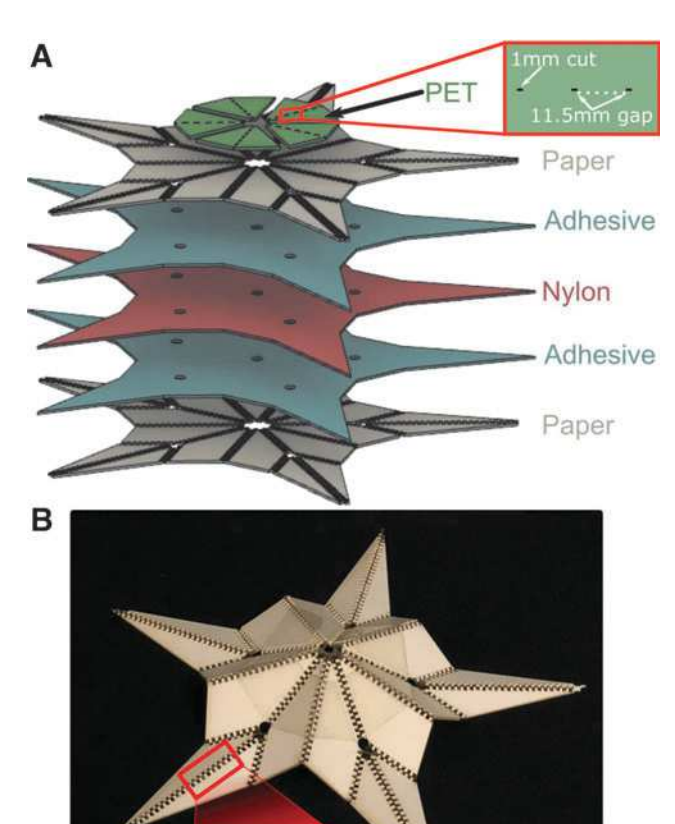


FIG. 2. Paper leaf-out prototype fabrication by layer. (A) Layout of the composite structure consisting of paper, adhesive, nylon, and PET layers. The layers also showcase the unique cut pattern required at each step of the process. (B) The photograph shows one of our handcrafted prototypes. The *inset* shows the magnified view of our comb-like crease design. PET, polyethylene terephthalate. Color images are available online.

20 mm

shows the layout of our leaf-out origami prototype composed of six layers stacked in the vertical direction. We use construction paper (Strathmore 500 Series 3-PLY BRISTOL; thickness of the paper is 0.5 mm) and nylon (thickness of 0.025 mm) to maintain the flat surfaces on each unit cell, and polyethylene terephthalate (PET; thickness of 0.25 mm) to define the rigidity along the crease lines, as seen in Figure 2A.

Between the bottom layer of the construction paper and the nylon, we use a 3M very high bond adhesive, and between the nylon and top layer of construction paper we use an archival double tack adhesive (ADTA). The ADTA covering is left along each crease line during the top construction paper layer cut because the prototypes are fabricated by being stacked, and so, the covering protected the nylon layer from being pierced by the laser during the cut for the top construction paper layer. The ADTA is used for the top layer adhesive because it is thicker and therefore more protective, as well as being less adhesive and easier to remove after the final cut for the structure is completed.

Figure 2B shows the fabricated prototype whose design parameters are $(n_{\text{cell}}, L_1, L_2) = (5, 70 \text{ mm}, 30 \text{ mm})$. To achieve

a sharp and straight crease folding, we introduce a comb-like crease design (see inset, Fig. 2B and also Supplementary Movie S1 for the folding behavior), which also helps to improve the consistency of folding behavior and to enhance the repeatability of tests. Without the PET layer, the structure's crease line stiffness is defined primarily by the flexible nylon layer. To increase the bending rigidity, the PET layer consisting of 1 mm cuts with 11.5 mm gaps in between each cut (see Fig. 2A for visualization) is applied, and the crease line stiffness is assumed to be defined solely by the PET layer due to the pliability of nylon. We found that tuning the stiffness of only the boundary edges, and leaving the other crease lines to be defined solely by the nylon layer, maximized the structure's ability to grasp onto dropped objects.

To analyze the folding/unfolding motion of the creases, we perform cyclic loading tests (100 cycles) on crease samples (Supplementary Fig. S1B). We use the loading curve from the last (100th) cycle to obtain the torsion spring constant per unit crease width ($\kappa_{\text{PET}} = 0.76 \text{ Nm/rad/mm}$). Using this normalized torsional spring constant, we adjust the torsional stiffness of the crease line in proportion to its length. The rest angle is $\bar{\rho} = 71.8^{\circ}$ based on the rigid crease model. While this angle is set manually in our study, it can be tuned by changing the materials, geometrical configurations, and/or preprocesses (e.g., oven heating) of our leaf-out architectures. We only use the thin nylon sheet as an elastic hinge for the creases without PET, resulting in creases with negligible stiffness. Therefore, we neglect the effect of the creases without PET in our analysis (i.e., $\kappa_M = \kappa_S = 0$).

Drop test

To experimentally demonstrate the grasping motion, we conduct drop tests (see Supplementary Fig. S2 for the testing setup). To capture the grasping motion, we use a high-speed camera (Chronos, Kron Technologies) filming at 1052 frames per second. The object we drop is a polyurethane ball of mass $m_{\text{ball}} = 22.3 \text{ g}$ and volume $v_{\text{ball}} = 179.6 \text{ cm}^3$ ($R_{\text{ball}} = 3.5 \text{ cm}$). We place the leaf-out on top of an aluminum plate in front of the ball drop device, with drop height measured from the top of the aluminum plate to the bottom of the ball. The ball is pinched in place over the center of the leaf-out structure by pressure from a screw. To drop the ball with zero initial velocity, we simply unscrew the bolt to release the ball.

Results

Uniform grasping motion

In this section, we consider the uniform deployment/contraction, that is, all of the Miura-ori unit cells show identical folding motion ($\rho_{M,n} = \rho_M$ and $\rho_{B,n} = \rho_B$ for $n = 1, \ldots, n_{\text{cell}}$), which corresponds to the case where the leaf-out origami catches a spherical target object. To achieve this folding mode, we control $\Delta \rho_0$ depending on the posture of each Miura-ori unit cell, which is described by the Euler angle (ψ). We can obtain the folding angle along the main crease line ρ_M from the Euler angle ψ as follows⁹:

$$\tan \alpha = \frac{\sin \alpha \cos(\rho_M/2)}{\cos \alpha \cos \psi - \sin \alpha \sin \psi \sin(\rho_M/2)}.$$
 (12)

In addition, the rotation of the unit vector e_2 around the boundary crease b through the angle ρ_B is identical to the rotation of e_2 around i_3 through 2α for the uniform grasping

motion. The rotation around the vector \boldsymbol{b} can be expressed by using the Rodrigues rotation formula as follows:

$$R_b = I_3 + \sin(-\pi + \rho_B) \,\hat{b} + [1 - \cos(-\pi + \rho_B)] \,\hat{b}_2 \quad (13)$$

where

$$\hat{b} = \begin{bmatrix} 0 & -b_3 & b_2 \\ b_3 & 0 & -b_1 \\ -b_2 & b_1 & 0 \end{bmatrix}. \tag{14}$$

Also, the rotation around i_3 is expressed by

$$R_3 = \begin{bmatrix} \cos 2\alpha & -\sin 2\alpha & 0\\ \sin 2\alpha & \cos 2\alpha & 0\\ 0 & 0 & 1 \end{bmatrix}. \tag{15}$$

Therefore, we obtain $R_3e_2 = R_be_2$. By solving this equation numerically, together with Equation (12), we obtain the relationship between the folding angles $(\rho_M$ and $\rho_B)$ and the Euler angle ψ .

By feeding these folding angles ρ_M and ρ_B as a function of the Euler angle ψ into the rigid origami model, we perform the simulation for the grasping motion of the leaf-out origami with $n_{\text{cell}} = 5$. Figure 1C shows the folding path plotted in the 3D configuration space where the negative and positive Euler angle regimes correspond to the open and closed phases, respectively, and $\psi = 0$ indicates that the leaf-out is completely flat (see the inset illustrations in the figure).

Based on the kinematic analysis, we also analyze the energy landscape for the transformation from the open phase to the closed state by using the energy expression [Eq. (11)]. Assuming identical torsional stiffness for every crease line (i.e., $\kappa_j = \kappa$ for $j = 1, ..., N_{\text{Total}}$), we calculate the potential energy change as shown in Figure 1D. Here, the rest angles for the main and boundary crease liens are $(\bar{\rho}_M, \bar{\rho}_B) = (120^\circ, -30^\circ)$ for this calculation. In the figure, the two black triangles indicate the local minimum states, which are separated by the energy peak at the flat state $(\psi = 0^\circ)$.

Therefore, starting from the open phase, once the structure overcomes the energy barrier, it triggers the grasping motion transforming to the stable closed state. To maintain this grasping shape, our leaf-out origami does not require external energy input. This implies that the structure can initiate a change in state by utilizing the energy from the target object (e.g., kinetic energy of a falling object, as demonstrated later). This contrasts with the conventional soft robotic grippers with pneumatic actuation²³ and with other origami-based robotic grippers,^{24–27} which require power from a source supplemental to the object being grasped. However, without the addition of an actively controlled actuation system, leafout origami grippers are limited to catching objects with enough input energy to overcome the structure's bistable energy barrier.

The natural follow-up question: is the grasping motion tunable? In other words, can we tailor the energy landscape to control the energy barrier and locations of the energy

minima? To investigate the tunability of the grasping motion, we analyze the energy landscape for various configurations, specifically different rest angles. We assume $\bar{\rho}_M = -\bar{\rho}_B$, and then $\bar{\rho}_S$ is obtained from the folding angle relationships [Eq. (2)]. Also, we assume identical torsional stiffness (κ) for every crease line. Figure 3A shows the energy landscapes as a function of the rest angle ($\bar{\rho}_M$) and Euler angle (ψ). The energy curves of the leaf-out origami show the local maximum peak at $\psi=0^\circ$, which corresponds to the complete flat state, and the analysis result clearly shows two energetically lower states before/after this peak, that is, bistable origami. 13-15

In addition, these bistable energy curves can be tailored drastically by varying the rest angle $(\bar{\rho}_M)$. Leaf-out origami can exhibit not only tunable bistability, but also a monostable configuration, specifically if $\bar{\rho}_M = 0^\circ$, which corresponds to the case in which the leaf-out origami is initially in the flat state (see the gray-colored curve in Fig. 3A).

To further analyze the tunability of this origami structure, we characterize the energy barrier between two stable states, by defining the energy gaps (ΔE_g and ΔE_r) as shown in Figure 3B. Letting the energy ratio be $\xi = (\Delta E_g - \Delta E_r)/(\Delta E_g + \Delta E_r)$, we compare the energy levels at each stable state by controlling two rest angles, $\bar{\rho}_M$ and $\bar{\rho}_B$. The surface plot of the energy ratio (ξ) in Figure 3C shows the two different regions bounded by the dashed line, indicated $\xi = 0$, that is, the open and closed stable states show the exact same values of local minimum energy.

In the left lower region, ΔE_g is greater than ΔE_r (Fig. 3B), which means that if the origami starts from the open stable state and transits to the other, the energy difference $\Delta E_g - \Delta E_r$ is trapped in the system, which can be advantageous for applications involving impact. On the contrary, if $\Delta E_g < \Delta E_r$, less energy is required to trigger the transition from open to closed states, a feature that can be particularly useful for sensitive actuation.

Experimental demonstration

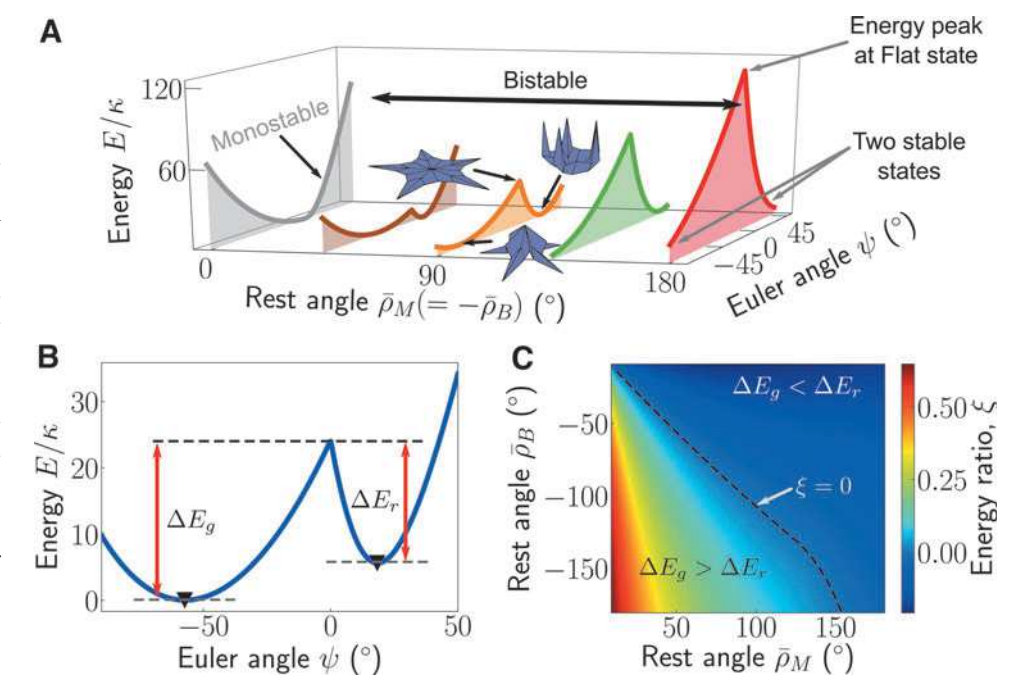
We examine the bistable energy landscape of our prototype by approximating the folding behavior of crease lines by a torsion spring. We use Equation (11) and construct the energy landscape of our actual prototype as shown in Figure 4A. The analysis result clearly indicates the two local minima in the potential energy plot, and each stable configuration of the leaf-out origami agrees qualitatively well with the postures of the actual prototype at its corresponding stable state.

To further validate the grasping based on bistability, specifically the energy barrier predicted by the rigid origami model, we conduct drop tests. Figure 4B shows the snapshots from the drop test in which the drop height is 360 mm. Our leaf-out origami prototype successfully demonstrates uniform grasping motion to capture and maintain hold of the target ball (see also Supplementary Movie S2 for the grasping motion of the prototype).

We analyze how the grasping motion can be triggered depending on the input, specifically the impact momentum, by varying the drop height. If the ball is dropped at the height h, the potential energy at the initial state is calculated as $E_{\text{ball}} = m_{\text{ball}}gh$ where g is the gravitational acceleration. Let $E_{\text{Gap}} = (E_{\text{ball}} - \Delta E_g)/\kappa_{\text{PET}}$. We plot this energy difference as a function of the drop height (h) and rest angle $(\bar{\rho})$. This is shown in Figure 4C, in which the dashed line indicates $E_{\text{Gap}} = 0$. If the drop height is below the threshold value (E_{Gap}) , the grasping motion is not triggered (denoted by the cross markers).

However, by crossing this boundary the leaf-out starts to overcome the energy barrier and transform into the closed phase (denoted by the circle markers). Note that if the impact momentum is too large, although the grasping motion is triggered, the leaf-out fails to retain the ball inside the structure (see Supplementary Movie S2 for this case). Although our paper prototype demonstrates the feasibility of

FIG. 3. Energy analysis. (A) Tailorable energy landscape altered by the rest angle $\bar{\rho}_M$. Here, we assume $\bar{\rho}_M =$ $-\bar{\rho}_{R}$, and $\bar{\rho}_{S}$ is obtained from the folding angle relationships (see Supplementary Data S1). **(B)** We characterize the asymmetric energy landscape by defining the energy gaps, ΔE_g and ΔE_r . $(\bar{\rho}_M, \bar{\rho}_B) =$ -120°) is used to calculate the potential energy curve. (C) Surface plot of the energy ratio, defined as $\xi = (\Delta E_g - \Delta E_r)/(\Delta E_g + \Delta E_r)$, as a function of two different rest angles $(\bar{\rho}_M, \bar{\rho}_B)$. Color images are available online.



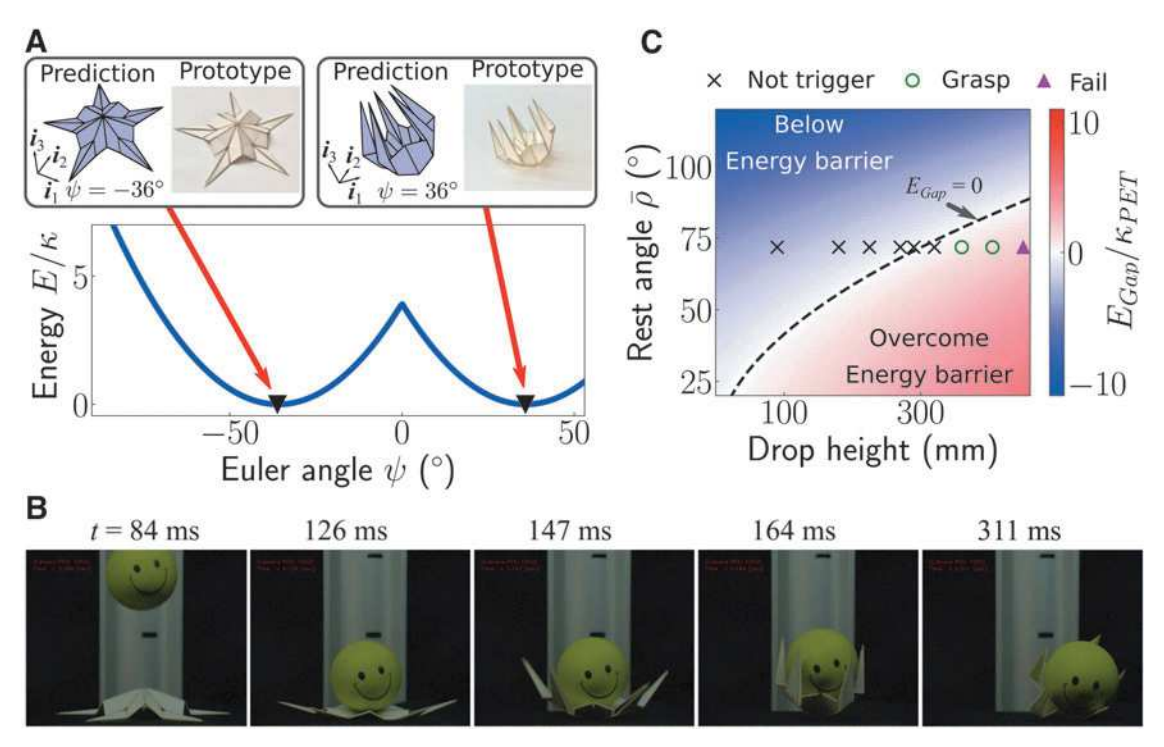


FIG. 4. Experimental demonstration of leaf-out origami grasping motion. (**A**) Bistable energy landscape for our paper prototype with PET hinges. The *left* and *right insets* show the comparison between the predicted configuration and the physical prototype for open and closed states, respectively. (**B**) Snapshots of the grasping motion of the leaf-out prototype from the high-speed camera images. The drop height is 360 mm. (**C**) We calculate the gap E_{Gap} between the energy barrier to trigger snap-through behavior (ΔE_g) and the potential energy E_{ball} (h) where h is the drop height. This energy gap is plotted as a function of the drop height (h) and the rest angle ($\bar{\rho}$) for the creases with PET. The *dashed line* indicates $E_{\text{Gap}} = 0$. The *cross*, *circle*, and *triangle* markers indicate the three different results of the drop test; (*cross* markers) the grasping motion was not triggered, (*circle*) the prototype grasped the ball, and (*triangle*) the grasping motion was triggered, but the prototype failed to hold the ball. Color images are available online.

grasping motion within a limited impact range, it suggests the potential of adaptive grasping *via* sensing the velocity and location of impact based on the carefully designed energy landscape (see Supplementary Movie S3 for off-center grasping).

Exploring multigrasping motions

One of the important tasks for grasping applications is to catch/hold an object even if its target shape varies from object to object. By leveraging the multi-DOF feature of the leaf-out origami, we show that the leaf-out can exhibit various grasping shapes. To explore different folding motions, we selectively control the main crease line of Miura-ori unit cells. In particular, we apply the controlled angle $(\Delta \rho_C)$ to the main folding angle of nth Miura-ori unit cell $(\rho_{M,n})$ in the arbitrary vector $\Delta \rho_0$, and then we perform the simulation to obtain the other main and boundary folding angles.

In our numerical analysis, we consider the leaf-out with $n_{\text{cell}} = 5$ to mimic human fingers, and we explore its various grasping motions. We start the simulations from the slightly folded configuration, specifically $(\rho_M^{(0)}, \rho_B^{(0)}) = (7.1^\circ, -3.6^\circ)$, to avoid the complete flat state, which hinders the mountain and valley crease assignments in the numerical calculations. Note that we maintain the mountain and valley

crease assignments in the simulations. Also, we use the identical $\Delta \rho_C$ for every controlled unit cell to simplify the analysis.

Figure 5A shows the simulation results for the two different cases as follows: (i) the first and second Miura-ori unit cells (n=1,2) are controlled, and (ii) first three unit cells (n=1,2,3) are controlled (see also Supplementary Movie S4 for the grasping animations). Unlike the uniform grasping motion (see the inset illustrations in Fig. 1D), the case where two unit cells (n=1,2) are controlled shows pinch-like folding motion of n=1 and 2 Miura-ori unit cells (analogous to a human hand pinching an object between the thumb and index fingers). Also, the leaf-out origami with three units controlled (n=1,2,3) exhibits an alligator-clip-like grasping motion, such as holding an object between three tips of n=1,2,3 unit cells and two tips of the other two (see the inset [ii] in Fig. 5A).

In addition, we examine the energy change during these two grasping motions, compared with the energy landscape for the uniform grasping motion. Here, $(\bar{\rho}_M, \bar{\rho}_B) = (60^\circ, -120^\circ)$ is used. In Figure 5B, the energy changes during grasping are plotted as a function of the controlled angle $(\Delta \rho_C)$, and the cases (i) and (ii) are denoted by the red and blue curves, respectively, as well as the uniform grasping case (gray curve). Our energy analysis clearly indicates the energy minimum state along all grasping paths.

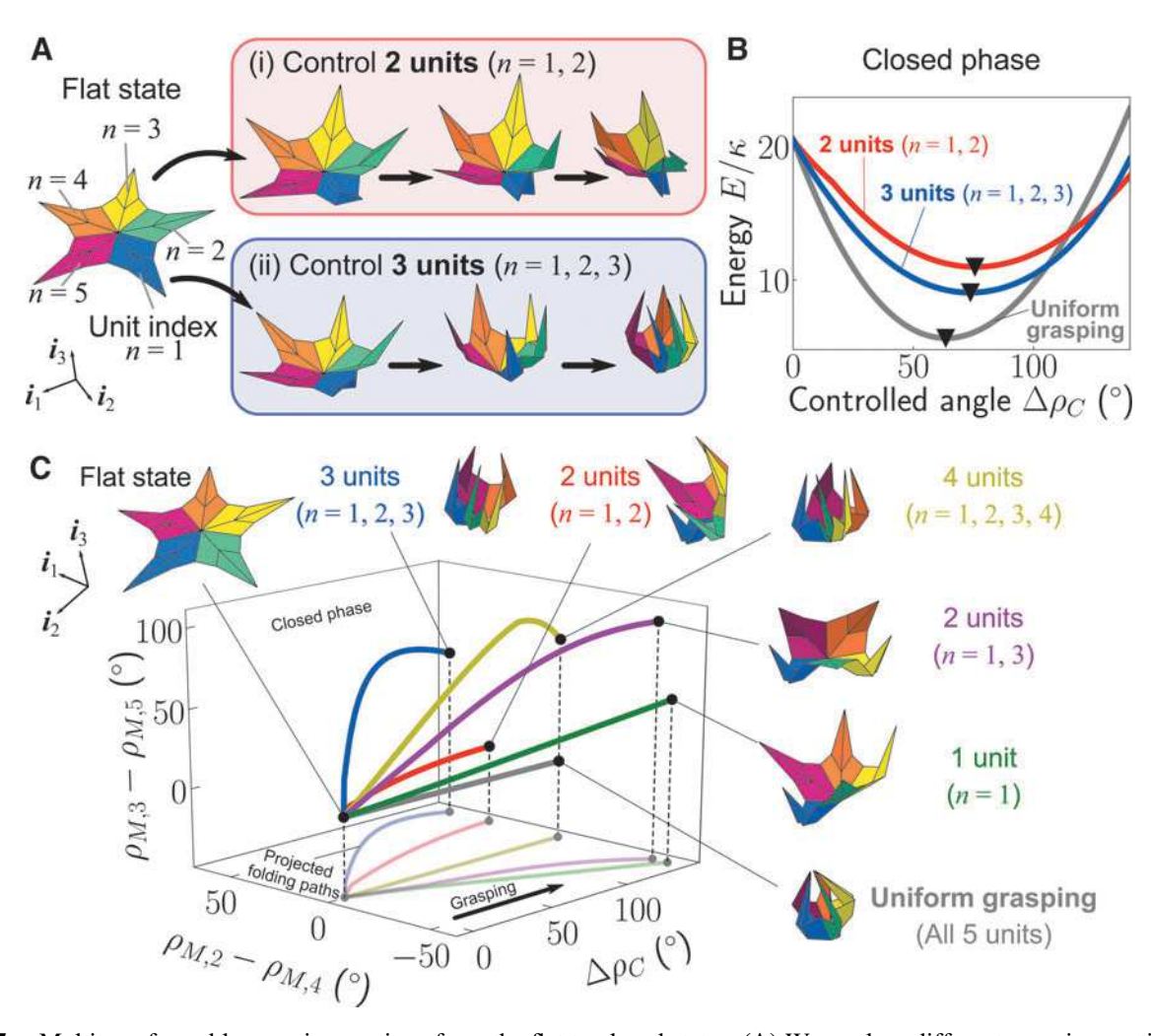


FIG. 5. Multitransformable grasping motions from the flat to closed states. (**A**) We explore different grasping motions by controlling the folding angles of (**i**) the two unit cells $(n=1, 2, i.e., \rho_{M,1} \text{ and } \rho_{M,2})$ and (**ii**) the three unit cells (n=1, 2, 3). (**B**) We calculate the energy landscapes for these two cases as well as the uniform grasping motion. The identical spring constant (κ) is used for all the crease lines, and $(\bar{\rho}_M, \bar{\rho}_B) = (60^\circ - 120^\circ)$ is used to calculate the energy curves. (**C**) Various different grasping motions are explored and plotted in the 3D configuration space. Each folding path is projected onto the *xy*-plane at the *bottom*. Color images are available online.

We further explore unique grasping motions by controlling different unit cells on the structure. Figure 5C shows three additional example motions and the three grasping motions discussed above (see Supplementary Movie S4 for each grasping motion). In this figure, by introducing two variables calculated by $\rho_{M,2}-\rho_{M,4}$ and $\rho_{M,3}-\rho_{M,5}$, we plot the folding paths in the configuration space as a function of $\Delta\rho_C$ to characterize different configurations of the leaf-out origami.

Interestingly, we find various folded shapes from our numerical simulations, particularly two controlled unit cases exhibiting different folding paths, and the final configurations depending on selected two unit elements (see the red and magenta curves in Fig. 5C for the two different cases of the leaf-out origami with n=1, 2 and n=1, 3 unit cells controlled). Note that these folding motions obtained from the rigid origami model are an example of possible folding motions by searching a valid configuration at each iteration step in the numerical calculation. Therefore, there are opportunities to achieve more diverse grasping modes in various ways, for example, using different controlled angles for dif-

ferent unit cells, enabling the reversal of mountain/valley creases, which can be useful for self-adaptive grasping for myriad target shapes.

Conclusion

We have numerically and experimentally studied the unique snap-through behavior of leaf-out origami for grasping devices. We have analyzed the multitransformable nature of the leaf-out structure by using a rigid origami model and found that the leaf-out origami structure exhibits a tailorable bistable energy landscape, enabling controllable snap-through behavior $\bar{\rho}_j$. To demonstrate the adaptive grasping motion of the leaf-out origami, we have designed and fabricated multilayered paper prototypes with customized hinges.

We have conducted drop tests by varying the drop height of a spherical target object, and our prototypes have exhibited controllable grasping motion through a triggering point that can be altered by the tailored energy landscape. In addition, we have explored various grasping motions by selectively controlling the unit cell components of the leaf-out origami, and our numerical results have suggested the potential for highly adaptive grasping motions for different target shapes, inspired by human hands and other examples from nature.

Due to the scale-independent nature of rigid origami structures, a grasping device based on the leaf-out design can be fabricated not only for centimeter-scale target objects but also for meter-scale applications (see Supplementary Fig. S3 and Supplementary Movie S5 for the grasping motion of the millimeter-scale prototype).

Leaf-out origami grippers can also be actively controlled by implementing low-power actuators at any scale, enabling power-constrained grasping robots to gather samples of various shaped objects. To fabricate the leaf-out origami, it will be interesting to consider different materials for various applications such as space structures and medical devices. In particular, soft materials can be beneficial to design a grasping device for fragile objects. From the numerical perspective, although we assumed that each surface remains flat during folding/unfolding in the present work, considering the surface deformations in the origami model would also be of interest to pursue. This study elucidates the potential applications of the leaf-out origami structure as a capture mechanism within systems that require lightweight, easily tunable, and autonomous grasping.

Acknowledgments

We thank Professors Sawyer Fuller and Shyam Gollakota for their help with the fabrication of the millimeter-scale Leaf-out prototype.

Author Disclosure Statement

No competing financial interests exist.

Funding Information

Jinkyu Yang and Hiromi Yasuda are also grateful for the support from the U.S. National Science Foundation (1553202 and 1933729) and the Washington Research Foundation. Hiromi Yasuda and Jordan R. Raney gratefully acknowledge support from the Army Research Office award number W911NF-17-1-0147 and the Air Force Office of Scientific Research award number FA9550-19-1-0285. Kyle Johnson thanks the Department of Education's Ronald E. McNair Postbaccalaureate Achievement Program, the National Science Foundation's Research Experience for Undergraduates program, and the Washington Research Foundation for their support. Koshiro Yamaguchi is supported by the Funai Foundation for Information Technology.

Supplementary Material

Supplementary Data S1

Supplementary Figure S1

Supplementary Figure S2

Supplementary Figure S3

Supplementary Movie S1

Supplementary Movie S2

Supplementary Movie S3

Supplementary Movie S4

Supplementary Movie S5

References

- Zang H, Liao B, Lang X, et al. Bionic torus as a selfadaptive soft grasper in robots. Appl Phys Lett 2020;116: 023701
- Guo Q, Dai E, Hang X, et al. Fast nastic motion of plants and bioinspired structures. J R Soc Interface 2015;12: 20150598.
- 3. Mu J, Wang G, Yan H, *et al.* Molecular-channel driven actuator with considerations for multiple configurations and color switching. Nat Commun 2018;9:590.
- Miura K. Method of packaging and deployment of large membranes in space. Inst Space Astronaut Sci Rep 1985; 618:1–9.
- 5. Kobayashi H, Kresling B, Vincent JFV. The geometry of unfolding tree leaves. Proc R Soc B Biol Sci 1998;265:147.
- De Focatiis DSA, Guest SD. Deployable membranes designed from folding tree leaves. Philos Trans A Math Phys Eng Sci 2002;360:227.
- Mahadevan L, Rica S. Self-organized origami. Science 2005;307:1740.
- 8. Faber JA, Arrieta AF, Studart AR. Bioinspired spring origami. Science 2018;359:1386.
- Yasuda H, Chen Z, Yang J. Multi-transformable leaf-out origami with bistable behavior. J Mech Robot 2016;8: 031013.
- 10. Hanna BH, Lund JM, Lang RJ, *et al.* Waterbomb base: a symmetric single-vertex bistable origami mechanism. Smart Mater Struct 2014;23:094009.
- 11. Treml B, Gillman A, Buskohl P, *et al.* Origami mechanologic. Proc Natl Acad Sci U S A 2018;115:6916.
- 12. Waitukaitis S, Menaut R, Chen BG-G, *et al.* Origami multistability: from single vertices to metasheets. Phys Rev Lett 2015;114:055503.
- 13. Jianguo C, Xiaowei D, Ya Z, *et al.* Bistable behavior of the cylindrical origami structure with Kresling pattern. J Mech Des 2015;137:061406.
- 14. Fang H, Li S, Ji H, *et al.* Dynamics of a bistable Miuraorigami structure. Phys Rev E 2017;95:052211.
- 15. Kamrava S, Mousanezhad D, Ebrahimi H, *et al.* Origami-based cellular metamaterial with auxetic, bistable, and self-locking properties. Sci Rep 2017;7:46046.
- Riley KS, Ang KJ, Martin KA, et al. Encoding multiple permanent shapes in 3D printed structures. Mater Des 2020;194:108888.
- 17. Lerner E, Zhang H, Zhao J. Design and experimentation of a variable stiffness bistable gripper. In: 2020 IEEE/RSJ International Conference on Intelligent Robots and Systems (IROS). 2020, pp. 9925–9931.
- 18. Jeong HY, An SC, Lim Y, *et al.* 3D and 4D printing of multistable structures. Appl Sci 2020;10:1–17.
- 19. Chen T, Bilal OR, Shea K, *et al.* Harnessing bistability for directional propulsion of soft, untethered robots. Proc Natl Acad Sci U S A 2018;115:5698–5702.
- Nishikawa S, Arai Y, Niiyama R, et al. Coordinated use of structure-integrated bistable actuation modules for agile locomotion. IEEE Robot Autom Lett 2018;3:1018– 1024.
- 21. Tachi T, Peters AK. Simulation of Rigid Origami. Natick, MA: R. J. Lang, 2009.
- 22. Tachi T. Proceedings of the International Association for Shell and Spatial Structures (IASS) Symposium: Geometric considerations for the design of rigid origami structures. Shanghai, China, 2010, pp. 771–782.

 Truby RL, Wehner M, Grosskopf A, et al. Soft somatosensitive actuators via embedded 3D printing. Adv Mater 2018;30:1706383.

- Edmondson BJ, Bowen LA, Grames CL, et al. Oriceps: origami-inspired forceps. In: Proceedings of the ASME 2013 Conference on Smart Materials, Adaptive Structures and Intelligent Systems. 2013.
- 25. Mintchev S, Shintake J, Floreano D. Bioinspired dual-stiffness origami. Sci Robot 2018;3:eaau0275.
- 26. Li S, Stampfli JJ, Xu HJ, *et al.* A vacuum-driven origami 'magic-ball' soft gripper. Proc IEEE Int Conf Robot Autom 2019;2019;7401–7408.

27. Hu F, Wang W, Cheng J, *et al.* Origami spring-inspired metamaterials and robots: an attempt at fully programmable robotics. Sci Prog 2020;103:0036850420946162.

Address correspondence to:
Jinkyu Yang
Department of Aeronautics & Astronautics
University of Washington
Seattle, WA 98195-2400
USA

E-mail: jkyang@aa.washington.edu